The Canadian Mineralogist
Vol. 53, pp. 803-820 (2015)
DOI: 10.3749/canmin.1400088

FONTARNAUITE, $(Na,K)_2(Sr,Ca)(SO_4)[B_5O_8(OH)](H_2O)_2$, A NEW SULFATE-BORATE MINERAL FROM DOĞANLAR (EMET), KÜTAHYA PROVINCE, WESTERN ANATOLIA, TURKEY

MARK A. COOPER AND FRANK C. HAWTHORNE

Department of Geological Sciences, University of Manitoba, 125 Dysart Road, Winnipeg, Manitoba R3T 2N2, Canada

JAVIER GARCÍA-VEIGAS AND XAVIER ALCOBÉ

Centres Cientificotècnics, Universitat de Barcelona, E-08028 Barcelona, Spain

CAHIT HELVACI

Dokuz Eylül Üniversitesi, Jeoloji Mühendisliği Bölümü, Tınaztepe Kampüsü, 35160 Buca-İzmir, Turkey

EDWARD S. GREW§

School of Earth and Climate Sciences, 5709 Bryand Global Sciences Center, University of Maine, Orono, Maine 04469, USA

NEIL A. BALL

Department of Geological Sciences, University of Manitoba, 125 Dysart Road, Winnipeg, Manitoba R3T 2N2, Canada

ABSTRACT

Fontarnauite was discovered in cores recovered from the Kütahya-Emet 2 and 188 (named here as Doğanlar) boreholes drilled in the Emet borate basin near the village of Doğanlar, Kütahya Province, Western Anatolia, Turkey. The Emet (or Emet-Hisarcık) basin is one of the Neogene basins in western Turkey bearing a borate-rich unit intercalated with Miocene sediments. Fontarnauite is most commonly associated with probertite, glauberite, and celestine and occurs as isolated colorless to light-brown prismatic crystals or as clusters of crystals less than 5 mm long. Fontarnauite is brittle, with a Mohs hardness of 2½–3, and perfect {010} cleavage. $D_{calc} = 2.533$ g/cm^3. The new mineral is optically biaxial (–), α 1.517(2), β 1.539(2), γ 1.543(2) (590 nm); $2V_{meas} = 46(1)°$; $2V_{calc} = 46°$; $X \wedge a$ 95.0° (β obtuse); $Y//b$, $Z \wedge c$ 81.9° (β acute). Dispersion is $r > v$, medium to weak. The chemical composition (electron microprobe; B and H from the crystal-structure refinement) is as follows: SO_3 17.75, B_2O_3 38.66, CaO 2.26, SrO 18.98, Na_2O 12.65, K_2O 1.70, H_2O 10.01, total 102.01 wt.%. The empirical formula (based on 15 O atoms per formula unit) is $(Na_{1.84}K_{0.16})_{\Sigma 2.00}(Sr_{0.82}Ca_{0.18})_{\Sigma 1.00}S_{1.00}B_5H_5O_{15}$; the endmember formula is $Na_2Sr(SO_4)[B_5O_8(OH)](H_2O)_2$ based on the crystal-structure refinement. Single-crystal X-ray studies gave the space group $P2_1/c$, a 6.458(2), b 22.299(7), c 8.571(2) Å, β 103.047(13)°, V 1202.5(1.0) Å^3, $Z = 4$. Structure refinement ($R1 = 2.9\%$) revealed that two BO_4 tetrahedra and three BO_3 triangles share vertices to form $B_5O_{10}(OH)$ units that link to other $B_5O_{10}(OH)$ units along [100] and [001] to give a $[B_5O_8(OH)]$ sheet parallel to (010). Within the central cavities of opposing sheets are the H_2O groups, SO_4 tetrahedra, and *Na*(1) sites; the *Sr* and *Na*(2) sites occupy the interstices of a given sheet. The region of the structure where opposing cusps of neighboring sheets approach each other is dominated by weaker H-bonding associated with the OH and H_2O groups, in accord with the observed perfect {010} cleavage. The strongest lines in the powder X-ray diffraction pattern, obtained after profile fitting using the Le Bail method, are as follows [d in Å (I) (hkl)]: 11.1498 (100)(020), 3.3948 (8)(061), 3.3389 (20)(042), 3.1993, 3.1990 (10)(160,$\bar{1}$42), 3.0458(10)(052), 3.0250(7)(220), 2.7500 (10)($\bar{2}$22,142), 2.3999 (8)(260), 2.2300, 2.2284(7)(0 10 0,222), 1.9241, 1.9237(7)(311,$\bar{2}$24). The holotype is deposited in the mineralogy collection of the Royal Ontario Museum, 100 Queen's Park, Toronto, Ontario M5S 2C6, Canada, accession number M56745.

Keywords: fontarnauite, new mineral, borate-sulfate, crystal structure, Emet borate basin, western Anatolia, Turkey.

§ *Corresponding author e-mail address*: esgrew@maine.edu

Introduction

Fontarnauite, $Na_2Sr(SO_4)[B_5O_8(OH)](H_2O)_2$, is the eighth borate-sulfate mineral found to date. Its structure is based on the distinctive $B_5O_8(OH)$ sheet composed of both trigonally and tetrahedrally coordinated boron. The structures of sedimentary borate minerals are of interest with regard to the relation between crystal structure and environment of crystallization. All sedimentary borate minerals contain only six borate clusters embedded in their structures, and these clusters are also the principal borate complexes occurring in aqueous solution (Hawthorne *et al*. 2002). This correlation suggests a mechanism for the crystallization of minerals from aqueous solutions, whereby crystallization proceeds by condensation of complex oxyanions in solution (Hawthorne 1979, 1983, Schindler & Hawthorne 2001a, b, c). In turn, this suggests a strong relationship between the pH of the environment of crystallization and the identity and proportions of borate clusters constituting the structures of specific minerals (Hawthorne 2012, 2014).

Fontarnauite was discovered in 2009 in cores recovered from the borate-bearing Miocene Emet basin in Western Anatolia, Turkey (García-Veigas *et al*. 2010, 2011). The mineral is named after Dr. Ramon Fontarnau i Griera (1944–2007), formerly Director of the Material Characterization Laboratory of the Serveis Cientificotecnics (now Centres Cientificotècnics) of the Universitat de Barcelona, in recognition of his efforts to promote the development of scientific facilities focused on, *inter alia*, mineral characterization. The mineral and its name have been approved by the International Mineralogical Association, Commission on New Minerals, Nomenclature and Classification (IMA no. 2009-64a). The holotype is deposited in the mineralogy collection of the Royal Ontario Museum, 100 Queen's Park, Toronto, Ontario M5S 2C6, Canada, accession number M56745.

In the present paper, we not only describe fontarnauite as a new mineral, but also compare it to other borate-sulfate minerals and to other borates containing the $B_5O_8(OH)$ sheet.

Occurrence

Fontarnauite was recovered from the Kütahya-Emet 2 and 188 (named here as Doğanlar) boreholes drilled in the Emet (or Emet-Hisarcık) basin near the village of Doğanlar, Kütahya Province, Western Anatolia, Turkey (García-Veigas *et al*. 2010, 2011). The Emet borate basin is one of the largest Neogene basins in western Turkey (Helvacı 1986, Helvacı & Ortí 1998). The basin sediments overlie Paleozoic metamorphic rocks. The sedimentary units of the Emet borate district consist, in ascending order, of a thin-bedded lower limestone with lenses of marl and tuffs; a red bed unit with coal and gypsum bands; a volcanoclastic sedimentary unit composed of clays and tuffaceous (pyroclastic) layers containing borates; and an upper limestone, all of Miocene age (Helvacı & Alonso 2000).

The exploration holes were drilled during 2003 in the area to the north of the Hisarcık open-cut mine in Quaternary alluvium of the Kocaçay River. The distance between the two boreholes is about 1.8 km. Borehole 2 is 716 m in depth, and fontarnauite was observed between 530 and 581.5 m depth; borehole 188 (516 m in depth) yielded fontarnauite between 249 and 351.9 m.

Fontarnauite is most commonly associated with probertite, glauberite, and celestine (Figs. 1–3). In addition, García-Veigas *et al*. (2011) reported fontarnauite with (1) halite, (2) kaliborite replacing probertite, and (3) kalistrontite, which replaced fontarnauite in pseudomorphs after glauberite. Other minerals occurring in the boreholes, most abundantly colemanite, ulexite, dolomite, arsenopyrite, realgar, and orpiment, have not been found with fontarnauite.

Fontarnauite is interpreted to be an early diagenetic phase, replacing both probertite (Figs. 1–4) and glauberite, as a consequence of the K-SO_4-enriched composition in residual brines during evaporation in a saline lake environment to which volcaniclastic material had been added. The age of fontarnauite crystallization is inferred to be 15 Ma, which is the age determined by K-Ar dating of the youngest volcanic rock interbedded with the borate unit in the Emet district (Helvacı & Alonso 2000).

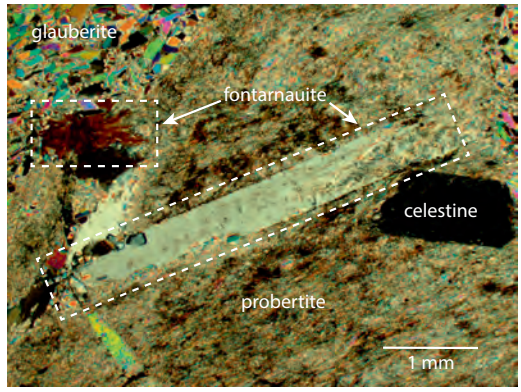

Fig. 1. Photomicrograph of prismatic fontarnauite crystals elongate along [100] (crossed polars). [Modification of figure used by permission of José Manuel Astilleros, Director of the journal *Macla*, from García-Veigas *et al*. (2010), Macla 13, Fig. 3, p. 98].

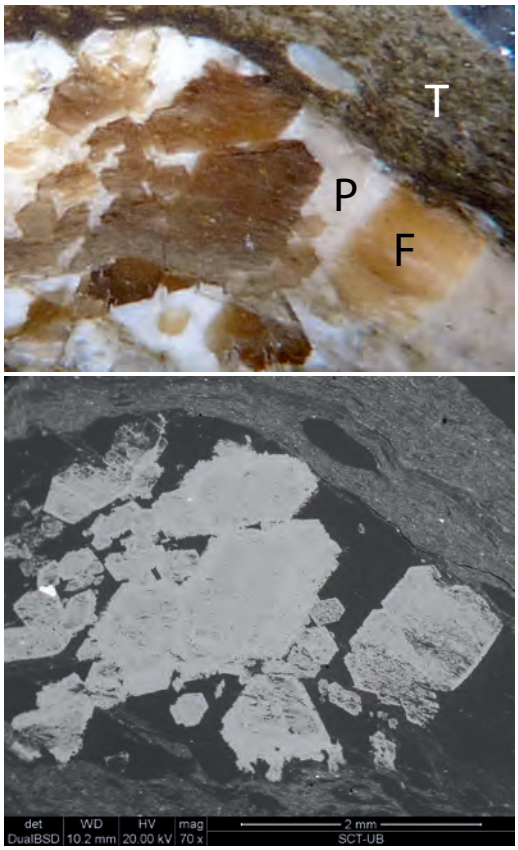

FIG. 2. Photomicrograph (upper) and BSE-SEM (lower) images of a cluster of fontarnauite crystals (F) in probertite (P) in the holotype sample. Faces on the six-sided crystals are the {010} side pinacoid and the {011} prism. T – tuff. [Used by permission of José Manuel Astilleros, Director of the journal *Macla*, from García-Veigas *et al*. (2010), Macla 13, Fig. 1, p. 97].

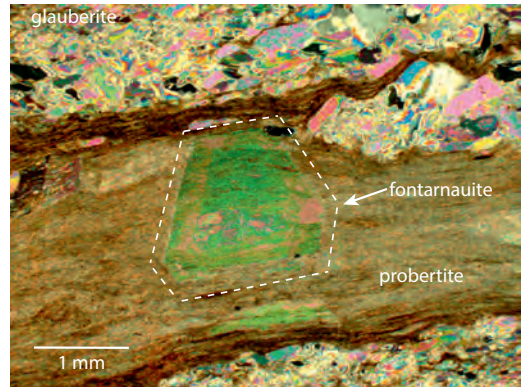

FIG. 3. Photomicrograph of fontarnauite crystals with hexagonal outline formed from the {010} side pinacoid and the {011} prism (crossed polars).

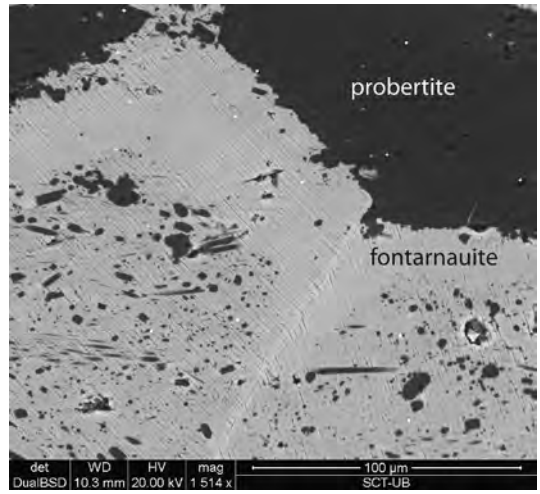

FIG. 4. BSE-SEM image of fontarnauite crystals showing the perfect {010} cleavage and abundant probertite inclusions. [Used by permission of José Manuel Astilleros, Director of the journal, *Macla*, from García-Veigas *et al*. (2010), Macla 13, Fig. 2, p. 97].

Overall, the eight known sulfate-borate minerals (Table 1) are relatively rare; most have been found at one or two localities worldwide, whereas sulfoborite and charlesite are reported from five localities or more. Four sulfate-borate minerals are found as late-stage products in deposits, such as the metamorphosed zinc deposits in Franklin, New Jersey (charlesite, Dunn *et al*. 1983); Wessels-type manganese ore, Kalahari field, South Africa (charlesite and sturmanite, Cairncross & Beukes 2013); and boron-rich skarns in the Solongo deposit, Buryatia, Russia (buryatite, Malinko *et al*. 2001; vitimite, Chukanov *et al*. 2002), whereas martinite is a late-stage product in sodalite syenite xenoliths altered by hyperagpaitic fluids at Mont Saint-Hilaire, Quebec (McDonald & Chao 2007). Like fontarnauite, the other two minerals (sulfoborite and heidornite) occur in evaporites, but in different parageneses; for example, sulfoborite with anhydrite and halite, along with in most cases at least one borate mineral such as hydroboracite, boracite, and kaliborite in the Inder, Chelkar, and Zhilyanskoye deposits, Kazakhstan (Lobanova 1958, Pekov & Abramov 1993); and heidornite in the Zechstein of Germany with glauberite in a vug in anhydrite (Nordhorn, von Engelhardt *et al*. 1956); or in anhydrite with halite (Kohnstein quarry, Siemroth 2008). The relative

TABLE 1. SULFATE-BORATE MINERALS

Mineral	Formula	Selected references
Sulfoborite	$Mg_3(OH)[B(OH)_4]_2(SO_4)F$	Bücking (1893), Lobanova (1958), Giese & Penna (1983) [a], Pekov & Abramov (1993)
Heidornite	$Na_2Ca_3B_5O_8(OH)_2(SO_4)_2Cl$	von Engelhardt *et al.* (1956), Burzlaff (1967) [a], Siemroth (2008)
Charlesite [b]	$Ca_6Al_2(SO_4)_2B(OH)_4(OH,O)_{12}\cdot 26H_2O$	Dunn *et al.* (1983)
Sturmanite [b]	$Ca_6Fe^{3+}{}_2(SO_4)_{2.5}[B(OH)_4](OH)_{12}\cdot 25H_2O$	Peacor *et al.* (1983), Pushcharovsky *et al.* (2004) [a]
Buryatite [b]	$Ca_3(Si,Fe^{3+},Al)SO_4B(OH)_4(OH,O)_6\cdot 12H_2O$	Malinko *et al.* (2001)
Vitimite	$Ca_6B_{14}O_{19}(SO_4)(OH)_{14}\cdot 5H_2O$	Chukanov *et al.* (2002)
Martinite	$(Na,\square,Ca)_{12}Ca_4(Si,S,B)_{14}B_2O_{38}(OH,Cl)_2F_2\cdot 4H_2O$	McDonald & Chao (2007) [a]
Fontarnauite	$Na_2Sr(SO_4)[B_5O_8(OH)](H_2O)_2$	This paper [a]

[a] Structure refinement
[b] Ettringite group

scarcity of sulfate-borate minerals in evaporites is rather surprising, as borates are commonly found with gypsum or anhydrite (*e.g.*, Ortí *et al*. 1998), suggesting that factors other than availability of essential constituents play a role in stabilizing sulfate-borates.

Appearance, Physical, and Optical Properties

Fontarnauite occurs as isolated prismatic crystals (Fig. 1) or as clusters of crystals less than 5 mm long, but pseudo-hexagonal sections less than 1 mm across are more common (Figs. 2 and 3). Less common are branching aggregates of crystals. An investigation with a single-crystal X-ray diffractometer showed that the crystals are elongate along [100] and that the six-sided prisms are formed from a combination of the {010} side pinacoid and the {011} prism. No terminal faces were available for examination.

An attempt to measure density by pycnometry using small fragments of fontarnauite crystals gave 2.37 g/cm^3, significantly less than the density calculated using the empirical formula, 2.533 g/cm^3, most likely because of abundant included probertite, which has a density of 2.15 g/cm^3. Fontarnauite is brittle, has a perfect {010} cleavage (Fig. 4), the orientation of which was confirmed with single-crystal study, and a splintery fracture; parting was not observed. Its Mohs hardness is 2½–3. Fontarnauite is colorless to light brown; it has a white streak. It is translucent to transparent, with a pearly luster. Fluorescence was not observed. It is biaxial (–), α 1.517(2), β 1.539(2), γ 1.543(2) (590 nm); $2V_{meas} = 46(1)°$, $2V_{calc} = 46°$; dispersion: $r > v$, medium to weak. The crystallographic orientation is: $X \wedge a$ 95.0° (β obtuse), $Y//b$, $Z \wedge c$ 81.9° (β acute).

Infrared and Raman Spectroscopy; Thermal Analysis

Methods

The Fourier-transform infrared (FTIR) spectra of fontarnauite were recorded at several temperatures with an IR-Plan Spectra Tech microscope joined to a FTIR Bomen MB-120 spectrometer in the Centres Cientificotècnics, Universitat de Barcelona. The spectra were obtained from small cleavage sheets crushed in a diamond-cell holder.

Raman spectra of fontarnauite were obtained from polished thin-sections using a Microbeam laser Raman spectrometer (Jobin Yvon T64000) with an Ar laser at 514.5 nm in the Centres Cientificotècnics, Universitat de Barcelona.

Simultaneous thermogravimetric (TG) and differential thermal (DT) analyses were carried out on small cleavage sheets of fontarnauite in the Centres Cientificotècnics, Universitat de Barcelona with an 851e/SF/1100 Mettler Toledo thermobalance in a N_2 gas environment, with a heating rate of 10 °C/min and using Al_2O_3 as reference material.

Results

The FTIR spectrum of fontarnauite at 25 °C (Fig. 5) shows a broad band with four or more overlapping peaks at 3587, 3531, 3404, and 3208 cm^{-1} assigned to O–H stretching modes. The peak at 1656 cm^{-1} is assigned to δ(H–O–H) bending. The strong peak at 1315–1365 cm^{-1} is assigned to asymmetric stretching for trigonally coordinated boron, $\nu_{as}(^{III}B–O)$, and that at 1136 cm^{-1}, to asymmetric stretching in tetrahedrally coordinated boron, $\nu_{as}(^{IV}B–O)$. The very strong peak at 989 cm^{-1} is due to symmetric stretching of the

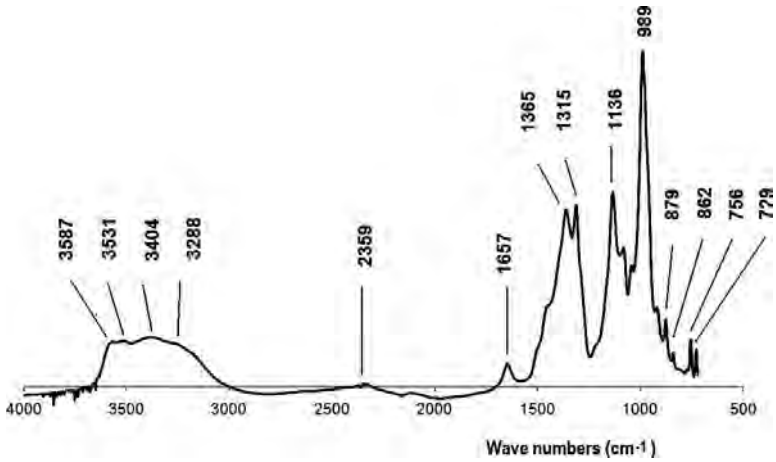

FIG. 5. FTIR spectrum of fontarnauite at 25 °C.

SO_4^{2-} group. The weak peak at 879 cm^{-1} is assigned to symmetric stretching for trigonally coordinated boron, $v_s(^{III}B–O)$, and the very weak peaks at 862 and 756 cm^{-1}, to symmetric stretching for tetrahedrally coordinated boron, $v_s(^{IV}B–O)$. The B–O frequencies are consistent with the presence of a complex polyanion containing both trigonal planar BO_3 units and tetrahedral BO_4 units (Li *et al*. 1995).

The Raman spectrum of fontarnauite (Fig. 6) shows the fundamental symmetric stretching vibration of the SO_4^{2-} group at 975 cm^{-1}. Two very weak peaks and a low intensity band (with two peaks) have been identified at 129, 160, and 430–470 cm^{-1}, respectively. Based on the peak assignments reported by Li *et al*. (1995), we suggest that the latter two peaks could be attributed to $^{IV}B–O$ bending, but the peaks for symmetric stretching of $^{IV}B–O$ and $^{III}B–O$ between 740 and 960 cm^{-1} appear to be obscured by intense fluorescence.

TG-DT analysis of small cleavage fragments of fontarnauite riddled with probertite and glauberite inclusions gave three endothermic peaks: between 25 and 350, between 450 and 620, and between 720 and 810 °C (Fig. 7). The total weight loss at 1000 °C is 14.39%. An FTIR spectrum of a sample heated at 350 °C showed that the first weight loss (9.5%) corresponds to partial dehydration. All H_2O is lost after heating at 650 °C. The total loss in weight attributed to H_2O is 12.1%, which exceeds the H_2O content calculated from the X-ray refinement. In contrast, the FTIR spectrum of a sample heated at 1000 °C shows that not all of the hydroxyl group was eliminated during heating.

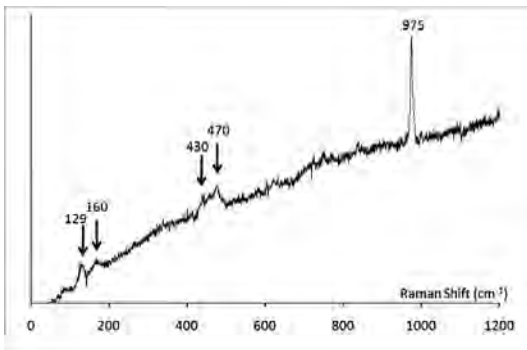

FIG. 6. Raman spectrum of fontarnauite.

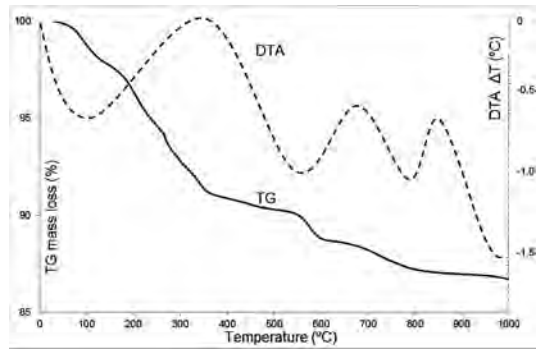

FIG. 7. Thermogravimetric (TG, solid line, axis to left) and differential thermal (DTA, dashed line, axis to right) analyses of fontarnauite in a sample from the Doğanlar 188 borehole at 249 m.

TABLE 2. CHEMICAL COMPOSITION OF FONTARNAUITE

	wt.%	Range	Standard deviation	Standard
B_2O_3	30.77	29.72–31.59	0.48	Boron
B_2O_3	38.66 [a]			
Na_2O	12.65	12.16–13.24	0.30	Albite
SO_3	17.75	17.00–18.20	0.26	Celestine
K_2O	1.70	0.87–2.20	0.44	Orthoclase
CaO	2.26	1.41–3.69	0.80	Wollastonite
SrO	18.98	16.47–20.94	1.58	Celestine
H_2O	10.01 [b]			
Total	102.01 [c]			

[a] Calculated from structure, B = 5.
[b] Calculated from structure, OH = 1, H_2O = 2.
[c] Includes structure B_2O_3 and H_2O contents, but not EMPA B_2O_3 content.

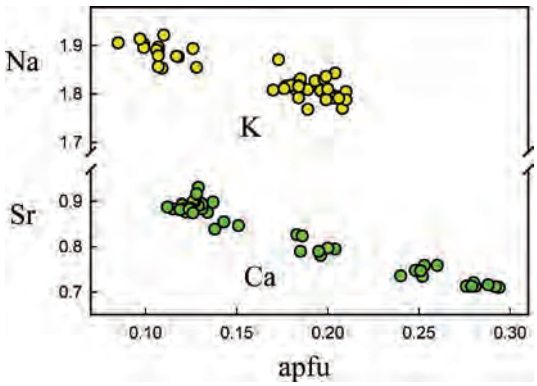

FIG. 8. Chemical variation in atoms per formula unit of Na *versus* K (yellow circles) and of Sr *versus* Ca (green circles) in fontarnauite in the holotype specimen.

CHEMICAL COMPOSITION

Chemical analyses (43) were done with a Cameca SX-50 electron microprobe (WDS mode, 15 kV, 6 nA, 10 μm beam diameter) at Centres Cientificotècnics, Universitat de Barcelona (Table 2). A special effort was made to analyze the material for boron using a Mo/B_4C layered synthetic crystal to improve analytical sensitivity (McGee *et al.* 1991). A significant shift in peak position between boron radiation in the pure boron crystal (used as a standard) and in analyzed minerals is required in order to optimize the background correction. Moderate energy (15 kV), low current (6 nA), large beam-diameter (10 μm), and a short counting time (10 s) were applied to avoid mobilization of boron and sodium. Matrix correction was done with the PAP routine (Pouchou & Pichoir 1988) integrated in the Cameca software. The B_2O_3 content determined with the electron microprobe and the H_2O content estimated by difference from 100 wt.% were used for the matrix correction. The improvement of PAP with a Mo/B_4C analyzer crystal over the ZAF method with a lead stearate crystal used by Hawthorne *et al.* (1995a) represents a more accurate determination of absorption effects. According to Bastin & Heijligers (2000), the problems of peak shape, peak shift, and crystallographic orientation in boron-bearing minerals can be mitigated using a good matrix-correction program in conjunction with a consistent set of mass-absorption coefficients. Analysis of probertite and kaliborite for B_2O_3 in the holotype specimen gave 15.1–16.1 wt.% (ideally 15.39 wt.%) and 17.7–19.0 wt.% (ideally 18.10 wt.%), respectively, giving an accuracy of better than 95% for this method. Nonetheless, the B_2O_3 content of fontarnauite determined by this method, 30.77 wt.%, is significantly lower than the structurally determined B_2O_3 content (Table 2), possibly because absorption of the B signal by Sr was not adequately corrected. The amount of H_2O was calculated by stoichiometry from the results of the crystal-structure analysis. The high total might be explained by a small loss of H_2O under the electron beam, which resulted in the other constituents appearing in higher concentrations than they actually are. This loss caused no visible damage to the sample surface.

The empirical formula (based on 15 O atoms per formula unit: *apfu*) is $(Na_{1.84}K_{0.16})_{\Sigma 2.00}(Sr_{0.82}Ca_{0.18})_{\Sigma 1.00}S_{1.00}B_5H_5O_{15}$, which can be simplified to $(Na,K)_2(Sr,Ca)(SO_4)[B_5O_8(OH)](H_2O)_2$. The end-member formula is $Na_2Sr(SO_4)[B_5O_8(OH)](H_2O)_2$, which requires Na_2O 13.14, SrO 22.30, SO_3 17.23, B_2O_3 37.45, H_2O 9.69, total 100 wt.%.

Minor but significant K and Ca were measured over the ranges $K_{0.09}$–$K_{0.21}$ and $Ca_{0.11}$–$Ca_{0.29}$ *apfu* in all 43 chemical analyses by electron microprobe. The variation in K and Ca is plotted against Na and Sr, respectively, in Figure 8. A simple 1:1 relation is indicated for both the Na-K and Sr-Ca plots, suggesting simple homovalent exchange of K for Na and Ca for Sr, with greater Ca incorporation overall. The variation in K is plotted against the variation in Ca in Figure 9, and the data fall within a triangular field, suggesting that the greater Ca-for-Sr substitution may only occur for more K-rich fontarnauite crystals. The Ca and K content of the X-ray crystal (derived from site scattering) is plotted as the green star on Figure 9, and is close to the average (Ca,K) content of the 43 individual analyses (large-diameter red circle).

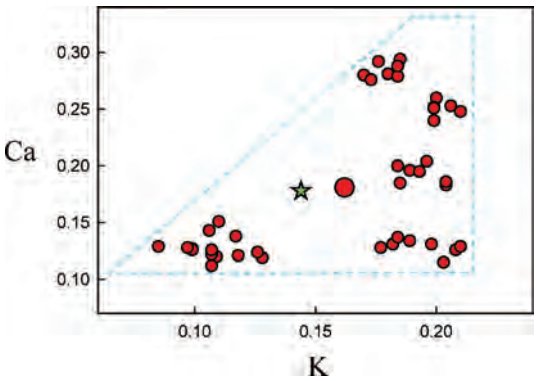

FIG. 9. Chemical variation in atoms per formula unit of Ca *versus* K in fontarnauite in the holotype specimen. Small red circles: 43 individual analyses; large red circle: average of the 43 individual analyses; green star: inferred Ca and K content deduced from structure refinement (see text). The near-coincidence of the average and refined compositions indicates that the structure crystal is representative of fontarnauite in the holotype specimen.

POWDER X-RAY DIFFRACTION

An X-ray powder-diffraction pattern was obtained using a PANalytical X'Pert PRO MPD powder diffractometer with Cu$K\alpha_1$ radiation ($\lambda = 1.5406$ Å) at the Centres Cientificotècnics, Universitat de Barcelona. The Cu$K\alpha_1$ radiation was selected with a primary Ge (111) Johansson-type monochromator. Diffraction data were collected with a linear position-sensitive silicon strip detector X'Celerator (active length 2.122° in 128 measuring channels). A minute amount of fontarnauite was mounted on a silicon single-crystal zero-background sample holder. A high-quality pattern was obtained with a θ/2θ scan from 3 to 80° 2θ, step size 0.017°, and 3420 seconds per step. As we worked with a linear position sensitive 1D detector of 2.122° of angular detection range (active length = 2.122° in 128 measuring channels), the total measuring time was 35.4 hours. The powder-diffraction pattern shows probertite as a minor phase. Observed peaks not assigned to probertite do not match any reported phase (International Centre for Diffraction Data 2012).

Indexing was started with DICVOL04 (Louër & Boultif 2006), taking into account all observed peaks except those assigned to probertite (García-Veigas *et al*. 2010). A monoclinic cell was found, and the space group was determined, taking into account the systematic absences. To check the cell parameters and the space group, a profile pattern-matching fitting procedure was done using the Le Bail method (Le Bail *et al*. 1988) and the FullProf program (Rodriguez-Carvajal 1997). The calculated X-ray powder-diffraction pattern for probertite, with a known crystal-structure (Menchetti *et al*. 1982), was considered in the fitting procedure. Figure 10 depicts the profile-fitting plot; it shows good correspondence between the observed and the calculated pattern. X-ray powder-diffraction data (in Å for Cu$K\alpha_1$) are given in Table 3.

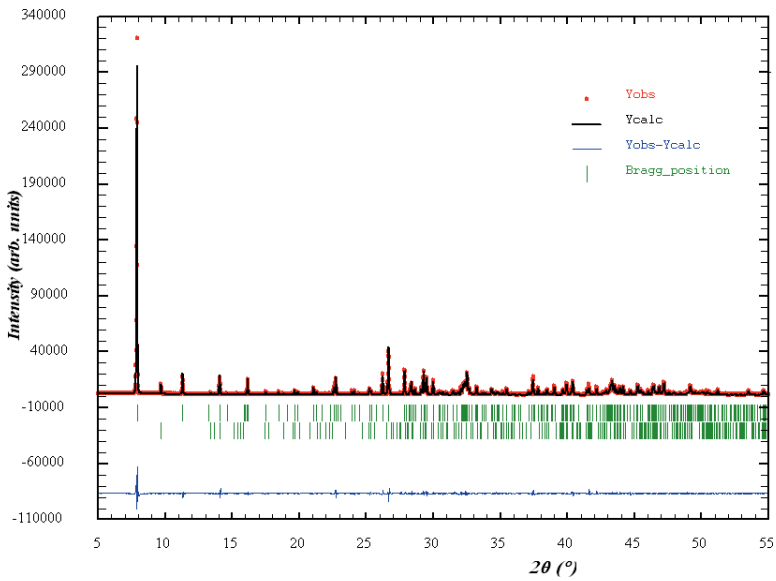

FIG. 10. Profile fitting plot. The first line of Bragg position peaks corresponds to fontarnauite. The second line corresponds to probertite.

TABLE 3. POWDER X-RAY DATA FOR FONTARNAUITE

I (meas)	*d* (meas), Å.	*hkl*
1000	11.1498	020
65	7.8104	011
64	6.2859	100
53	5.4757	120
11	5.0579	$\bar{1}21$
10	4.7999	130
13	4.5110	$\bar{1}31$
9	4.4567	111
28	4.2115	121
12	4.1710, 4.1694	140, 002
28	3.9329	051
68	3.9060, 3.9053	$\bar{1}02$, 022
13	3.7167	060
17	3.6863	$\bar{1}22$
27	3.5243	141
14	3.5068	$\bar{1}51$
6	3.4577	$\bar{1}32$
78	3.3948	061
199	3.3389	042
102	3.1993, 3.1990	160, $\bar{1}42$
15	3.1569	$\bar{2}11$
55	3.1429	200
25	3.1121	210, $\bar{1}61$
25	3.0661	$\bar{2}21$
100	3.0458	052
71	3.0250	220
58	2.9760	071
8	2.9385	$\bar{1}52$
13	2.9307	$\bar{2}31$
13	2.9084	132
25	2.8416	170, $\bar{2}02$
11	2.8150	$\bar{2}12$
28	2.7876	080
41	2.7744	062
10	2.7682	$\bar{2}41$
46	2.7648	$\bar{1}13$
26	2.7583	013
99	2.7500	$\bar{2}22$, 142
28	2.7378	240
7	2.7032	$\bar{1}23$
36	2.6926	$\bar{1}62$
10	2.6636	221
12	2.6511	$\bar{2}32$
6	2.6437	081
27	2.6094, 2.6091	171, $\bar{1}33$
8	2.6035	033
13	2.5941	$\bar{2}51$
15	2.5786	152
9	2.5691	250
14	2.5482	180
29	2.5290	$\bar{2}42$
7	2.5020	$\bar{1}81$
17	2.4203	$\bar{2}61$

TABLE 3. CONTINUED.

I (meas)	*d* (meas), Å.	*hkl*
8	2.4076	162
75	2.3999	260
36	2.3767, 2.3752	181, 091
10	2.3518	$\bar{2}13$
28	2.3365	251
8	2.3173	082
42	2.3052	190
28	2.2690	$\bar{1}82$
46	2.2555	$\bar{2}62$
15	2.2538, 2.2536	$\bar{2}71$, $\bar{2}33$
15	2.2374	270
72	2.2300, 2.2284	0 10 0, 222
29	2.1772, 2.1759, 2.1747	$\bar{2}43$, 191, 232
31	2.1675	143
7	2.1543	0 10 1
35	2.1406	$\bar{3}11$
12	2.1190, 2.1184	$\bar{2}72$, $\bar{1}14$
9	2.1116	$\bar{3}21$
26	2.1058	242
8	2.0988, 2.0973	$\bar{2}81$, $\bar{2}73$
10	2.0953, 2.0945	300, 073
14	2.0924	$\bar{1}92$
34	2.0905, 2.0903, 2.0894	182, $\bar{1}24$, $\bar{2}53$
13	2.0894	$\bar{2}53$
69	2.0861, 2.0855, 2.0847	310, 280, 004
45	2.0787	271
27	2.0697	$\bar{3}02$
36	2.0592	320
47	2.0492	024
27	2.0260	252
7	2.0072, 2.0064	034, $\bar{3}41$
52	2.0023	1 10 1
23	1.9953, 1.9939	263, $\bar{3}32$
20	1.9886, 1.9881, 1.9879	$\bar{2}82$, $\bar{1}44$, 163
22	1.9707, 1.9699	$\bar{1}83$, 0 11 1
39	1.9566	$\bar{2}91$, 281
38	1.9530, 1.9527	$\bar{2}04$, 044
14	1.9458, 1.9456	290, $\bar{2}14$
45	1.9371, 1.9366	$\bar{3}51$, $\bar{1}$ 10 2
6	1.9294	1 11 0
71	1.9241, 1.9237	311, $\bar{2}24$
20	1.9092	$\bar{1}$ 11 1
6	1.8989	$\bar{2}73$
12	1.8964	350
7	1.8925	173
12	1.8774	$\bar{3}52$
8	1.8614	$\bar{3}61$
10	1.8584	0 12 0
6	1.8551	223
51	1.8517, 1.8516, 1.8510, 1.8506	1 11 1, $\bar{1}93$, 272, 114
9	1.8467	$\bar{1}64$
7	1.8432	$\bar{2}44$
19	1.8387	291

TABLE 3. CONTINUED.

I (meas)	*d* (meas), Å.	*hkl*
6	1.8334	$\bar{3}33$
9	1.8318	124
7	1.8220	1 10 2
20	1.8187, 1.8182	2 10 0, 064
6	1.8139	0 12 1
21	1.8082	$\bar{3}62$

The reported *I* and *d* values are those obtained after profile fitting using the Le Bail method. Observed and calculated *I* and *d* values thus can be considered to be identical.

A Le Bail fit gave monoclinic symmetry, space group: $P2_1/c$; *a* 6.4536(1), *b* 22.3004(3), *c* 8.5615(1) Å, β 103.095(2)°, *V* 1200.11(3) Å^3, *Z* = 4, in good agreement with the values obtained from single-crystal X-ray diffraction.

Single-Crystal X-Ray Diffraction and Crystal Structure

Methods

A single-crystal fragment (20 × 50 × 100 μm) of fontarnauite was removed from a polished core section, attached to a tapered glass fiber, and then mounted on a Bruker D8 three-circle diffractometer equipped with a rotating-anode generator (Mo*K*α X-radiation), multilayer optics, and an APEX-II CCD area detector at the University of Manitoba (Table 4). A total of 46942 intensities (13879 in the Ewald sphere) was collected to $2\theta = 60°$ using a 20 s per 0.3° frame with a crystal-to-detector distance of 5 cm. Empirical absorption corrections (SADABS; Sheldrick 2008) were applied and equivalent reflections were merged, resulting in 3531 unique reflections. The unit-cell dimensions were obtained by least-squares refinement of the positions of 4085 reflections with $I > 10\sigma I$. The crystal structure of fontarnauite was solved by direct methods and refined in the space group $P2_1/c$ to an R_1 index of 2.9%; atom positions and equivalent-isotropic and anisotropic-displacement parameters are given in Tables 5 and 6, respectively, and selected interatomic distances and associated bond-valences (Brown & Altermatt 1985) are given in Tables 7 and 8.

Crystal structure: site populations

In the crystal structure of fontarnauite, the observed site-scattering (Hawthorne *et al*. 1995b) (= 16 e) at the *S* site and the <*S*–O> distance (1.473 Å) involving four tetrahedrally coordinated O atoms are consistent with full occupancy of the *S* site by S^{6+}, in accord with the measured S value from electron-microprobe analysis and the grand <S–O> distance of 1.478 Å in sulfate minerals (Hawthorne *et al*. 2000). There are five *B* sites, with observed scattering values of 5 *epfu* (electrons per formula unit) consistent with full occupancy by B. Moreover, the observed $<^{[3]}B–O>$ and $<^{[4]}B–O>$ distances of 1.369 and 1.475 Å, respectively, are in accord with the grand $<^{[3]}B–O>$ and $<^{[4]}B–O>$ distances of 1.370 and 1.476 Å, respectively, given by Hawthorne *et al*. (2002). Hence, five B *apfu* (atoms per formula unit) were inserted into the normalization of the chemical data.

There are three sites (each contributing 1 *apfu*) associated with larger coordination numbers ([6]–[10]) and greater mean bond-length (2.48–2.70 Å), that contain the larger cations $(Na_{1.84}Sr_{0.82}Ca_{0.18}K_{0.16})_{\Sigma 3}$. These cations increase in ionic radius in the sequence (Na ≈ Ca < Sr < K) and contain 11, 20, 38, and 19 electrons, respectively. The *Na*(2) site has the shortest

TABLE 4. EXPERIMENTAL DETAILS

Diffractometer	Bruker APEX-II ULTRA three-circle
X-ray radiation	Mo*K*α (0.71073 Å)
Crystal size (mm)	0.02 × 0.05 × 0.10
Space group	$P2_1/c$
Cell dimensions (Å)	$a = 6.458(2)$ $b = 22.299(7)$ $c = 8.571(2)$ $\beta = 103.047(13)°$
Cell volume (Å^3)	1202.5(1.0) Å^3
Refined formula	$(Na_{0.856}K_{0.144})Na(Sr_{0.822}Ca_{0.178})(SO_4)[B_5O_8(OH)](H_2O)_2$
Z	4
Reflections collected	46942
Reflections in Ewald sphere	13879
Max. 2θ	60°
Index range	$-9 \le h \le 9$ $-31 \le k \le 31$ $-12 \le l \le 12$
Unique reflections	3531
Reflections > 2σ(*I*)	3299
R_{merge}	0.018
No. least squares parameters	223
GooF	1.098
*R*1 , $I > 2\sigma(I)$	0.029
*R*1 , all data	0.032
w*R*2 (on F^2)	0.071
$\Delta\rho_{min}$ ($-e \cdot$ Å^{-3})	–0.70
$\Delta\rho_{max}$ ($e \cdot$ Å^{-3})	0.89

TABLE 5. ATOM POSITIONS AND DISPLACEMENT PARAMETERS (Å)^2 FOR FONTARNAUITE

Site	*x*	*y*	*z*	U_{eq}
Na(1)	0.93117(19)	0.35709(6)	0.67727(16)	0.0410(5)
Na(2)	0.0660(2)	0.45901(7)	0.3407(3)	0.0623(6)
Sr	0.45961(3)	0.26450(1)	0.98574(2)	0.01195(7)
S	0.43885(9)	0.36146(2)	0.70433(6)	0.01702(13)
B(1)	0.7146(4)	0.33219(10)	0.3047(3)	0.0110(4)
B(2)	0.0099(4)	0.30970(10)	0.1724(3)	0.0103(4)
B(3)	0.9768(4)	0.25430(10)	0.4174(3)	0.0110(4)
B(4)	0.3405(4)	0.37153(10)	0.2606(3)	0.0121(4)
B(5)	0.6325(4)	0.43729(11)	0.3636(3)	0.0141(4)
O(1)	0.3673(3)	0.36822(9)	0.8550(2)	0.0250(4)
O(2)	0.5586(3)	0.41411(8)	0.6731(2)	0.0237(4)
O(3)	0.5833(4)	0.30829(9)	0.7246(3)	0.0336(5)
O(4)	0.2597(4)	0.34965(13)	0.5701(3)	0.0479(7)
O(5)	0.7844(2)	0.32171(7)	0.15740(17)	0.0114(3)
O(6)	0.7736(2)	0.39189(7)	0.37577(18)	0.0137(3)
O(7)	0.8020(2)	0.28732(7)	0.43028(17)	0.0122(3)
O(8)	0.4788(2)	0.32425(7)	0.26631(18)	0.0125(3)
O(9)	0.0627(2)	0.28922(7)	0.02386(17	0.0132(3)
O(10)	0.1284(2)	0.36620(7)	0.21618(18)	0.0120(3)
O(11)	0.0812(2)	0.26271(7)	0.29630(18)	0.0129(3)
O(12)	0.4179(2)	0.42923(7)	0.3012(2)	0.0159(3)
OH	0.7119(3)	0.49302(7)	0.4120(2)	0.0197(3)
W(1)	0.9942(4)	0.45016(17)	0.8128(4)	0.0651(9)
W(2)	0.7322(4)	0.44312(12)	0.0357(3)	0.0448(6)
H(1)	0.614(7)	0.5270(16)	0.387(7)	0.11(2)

TABLE 6. ANISOTROPIC DISPLACEMENT PARAMETERS (Å)^2 FOR FONTARNAUITE

	U_{11}	U_{22}	U_{33}	U_{23}	U_{13}	U_{12}
Na(1)	0.0333(7)	0.0403(7)	0.0546(8)	0.0062(5)	0.0212(5)	0.0008(5)
Na(2)	0.0339(7)	0.0457(8)	0.1200(15)	–0.0490(9)	0.0443(9)	–0.0173(6)
Sr	0.00997(10)	0.01421(11)	0.01157(10)	–0.00080(7)	0.00221(7)	0.00018(7)
S	0.0204(3)	0.0159(2)	0.0141(2)	0.00052(18)	0.00258(19)	–0.00349(19)
B(1)	0.0076(9)	0.0125(9)	0.0131(9)	–0.0004(7)	0.0029(7)	0.0005(7)
B(2)	0.0089(9)	0.0128(9)	0.0090(9)	–0.0003(7)	0.0018(7)	0.0000(7)
B(3)	0.0096(9)	0.0128(9)	0.0107(9)	–0.0002(7)	0.0025(7)	–0.0004(7)
B(4)	0.0110(9)	0.0132(10)	0.0122(9)	–0.0012(8)	0.0031(7)	–0.0009(8)
B(5)	0.0123(10)	0.0136(10)	0.0167(10)	–0.0002(8)	0.0036(8)	–0.0011(8)
O(1)	0.0302(10)	0.0264(9)	0.0211(8)	0.0023(7)	0.0116(7)	0.0058(7)
O(2)	0.0213(8)	0.0180(8)	0.0313(9)	0.0050(7)	0.0048(7)	–0.0032(6)
O(3)	0.0571(14)	0.0180(8)	0.0325(10)	0.0031(7)	0.0247(10)	0.0091(9)
O(4)	0.0403(13)	0.0730(18)	0.0233(10)	0.0074(10)	–0.0076(9)	–0.0332(12)
O(5)	0.0086(6)	0.0144(7)	0.0111(6)	0.0002(5)	0.0024(5)	0.0004(5)
O(6)	0.0098(6)	0.0132(7)	0.0177(7)	–0.0031(5)	0.0026(5)	–0.0004(5)
O(7)	0.0110(7)	0.0143(7)	0.0123(6)	0.0014(5)	0.0047(5)	0.0028(5)
O(8)	0.0081(6)	0.0119(6)	0.0176(7)	–0.0019(5)	0.0031(5)	0.0000(5)
O(9)	0.0132(7)	0.0159(7)	0.0116(6)	–0.0031(5)	0.0048(5)	–0.0032(5)
O(10)	0.0082(6)	0.0124(7)	0.0150(7)	–0.0020(5)	0.0016(5)	–0.0002(5)
O(11)	0.0115(7)	0.0160(7)	0.0127(7)	0.0037(5)	0.0056(5)	0.0040(5)
O(12)	0.0095(7)	0.0119(7)	0.0250(8)	–0.0022(6)	0.0010(6)	0.0006(5)
OH	0.0144(7)	0.0129(7)	0.0309(9)	–0.0038(6)	0.0034(6)	–0.0023(6)
W(1)	0.0317(13)	0.109(3)	0.0557(17)	–0.0163(17)	0.0111(12)	–0.0134(15)
W(2)	0.0551(15)	0.0433(13)	0.0346(12)	0.0003(10)	0.0070(11)	–0.0127(11)

TABLE 7. SELECTED INTERATOMIC DISTANCES (Å) AND ANGLES (°) FOR FONTARNAUITE

S–O(1)	1.474(2)	*Na*(1)–O(1)	2.895(3)
S–O(2)	1.464(2)	*Na*(1)–O(2)	2.715(2)
S–O(3)	1.494(2)	*Na*(1)–O(3)	2.609(3)
S–O(4)	1.460(2)	*Na*(1)–O(4)	2.501(3)
<*S*–O>	1.473	*Na*(1)–O(6)	2.670(2)
		Na(1)–O(7)	2.608(2)
B(1)–O(5)	1.453(3)	*Na*(1)–O(11)	2.945(2)
B(1)–O(6)	1.478(3)	*Na*(1)–W(1)	2.368(4)
B(1)–O(7)	1.484(3)	<*Na*(1)–Φ>	2.664
B(1)–O(8)	1.494(3)		
<*B*(1)–O>	1.477	*Na*(2)–O(6)	2.481(2)
		Na(2)–O(10)	2.404(2)
B(2)–O(5)	1.458(3)	*Na*(2)–O(12)	2.463(2)
B(2)–O(9)	1.463(3)	*Na*(2)–OH	2.515(3)
B(2)–O(10)	1.478(3)	*Na*(2)–OH	2.610(2)
B(2)–O(11)	1.489(3)	*Na*(2)–W(1)	2.399(4)
<*B*(2)–O>	1.472	<*Na*(2)–Φ>	2.479
B(3)–O(7)	1.373(3)	*Sr*–O(1)	2.580(2)
B(3)–O(9)	1.362(3)	*Sr*–O(3)	2.594(2)
B(3)–O(11)	1.372(3)	*Sr*–O(3)	2.722(2)
<*B*(3)–O>	1.369	*Sr*–O(4)	3.015(2)
		Sr–O(5)	2.607(2)
B(4)–O(8)	1.375(3)	*Sr*–O(7)	2.632(2)
B(4)–O(10)	1.342(3)	*Sr*–O(8)	2.727(2)
B(4)–O(12)	1.396(3)	*Sr*–O(8)	2.752(2)
<*B*(4)–O>	1.371	*Sr*–O(9)	2.713(2)
		Sr–O(11)	2.681(2)
B(5)–O(6)	1.350(3)	<*Sr*–O>	2.702
B(5)–O(12)	1.380(3)		
B(5)–OH	1.372(3)	OH–O(2)	2.701(3)
<*B*(5)–Φ>	1.367	H(1)...O(2)	1.723(6)
		OH–H(1)–O(2)	175(6)

mean bond-length [(<*Na*(2)–O> = 2.479 Å)], the smallest coordination number [6], and a refined site-scattering of 11 *epfu*, consistent with full occupancy by Na. The *Na*(1) site has a mean bond-length of 2.664 Å, is coordinated by eight anions, and has a refined site-scattering value of 12.15(8) *epfu*; this is consistent with dominant occupancy by Na, in addition to a minor substituent(s) with more electrons (*i.e.*, K, Ca, or Sr). The ionic radii for these cations [coordination number (CN) = 8] is as follows: Na 1.18, K 1.51, Ca 1.12, Sr 1.26 Å (Shannon 1976). If we subtract a mean O radius of 1.37 Å from the observed value of 2.664 Å for the mean bond-length, we arrive at 1.29 Å for the aggregate cation radius. Of the available substituents (K, Ca, Sr), K is the only candidate large enough to increase the aggregate radius as required. We therefore assigned the Na and K scattering factors to the *Na*(1) site, and allowed their relative occupancies to refine

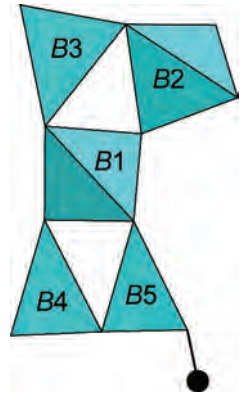

FIG. 11. The $[B_5O_{10}(OH)]$ unit in fontarnauite.

with the constraint that the site be fully occupied; this gave a refined site composition of $Na_{0.856}K_{0.144}$.

The Sr site has a mean bond-length of 2.702 Å, is coordinated by 10 anions, and has a refined site-scattering value of 34.80(7) *epfu*; this is consistent with dominant occupancy by Sr, in addition to a minor substituent(s) with fewer electrons (*i.e.*, Na, K, Ca). The ionic radius of these cations (CN = 10) is as follows: Na 1.28, K 1.59, Ca 1.23, Sr 1.36 Å. If we subtract a mean O radius of 1.37 Å from the observed mean bond-length of 2.702 Å, we arrive at 1.33 Å for the aggregate cation radius. Of the available substituents (Na, K, Ca), both Na and Ca are potential substituents whose presence would serve to reduce both the mean scattering (*i.e.*, below Sr = 38 *epfu*) and the aggregate radius (*i.e.*, to less than $^{[10]}Sr = 1.36$ Å). Let us examine these two possibilities: (1) Sr + Ca, or (2) Sr + Na at the *Sr* site. The observed refined site-scattering value of 34.80 *epfu* at the *Sr* site is compatible with the following cation occupancies: (1) $Sr_{0.822}Ca_{0.178}$ and (2) $Sr_{0.881}Na_{0.119}$. The Sr values measured by electron-microprobe analysis span 0.71–0.93 Sr *apfu*, and both Sr values arrived at from site-scattering arguments (*i.e.*, 0.822 *versus* 0.881 *apfu*) fall within the observed chemical composition. However, if we sum the Na content derived from the site-scattering over the three sites with the assumption of (Sr + Na) at the *Sr* site, we arrive at a Na sum of 1.975 *apfu* (*i.e.*, 0.856 $Na^{Na(1)}$ + 1 $Na^{Na(2)}$ + 0.119 Na^{Sr}), which exceeds the observed Na from chemical analysis (*i.e.*, 1.77–1.92 Na *apfu*); we also neglected to account for the observed Ca during chemical analysis (*i.e.*, 0.11–0.29 Ca *apfu*) and introduced an overall imbalance in charges (*i.e.*, $Sr_{0.881}Na_{0.119}$ < 2+). On the other hand, if we assign $Sr_{0.822}Ca_{0.178}$ to the *Sr* site, we produce excellent overall agreement between the observed site-scattering and observed

TABLE 8. BOND-VALENCE (vu) FOR FONTARNAUITE

	S	*B*(1)	*B*(2)	*B*(3)	*B*(4)	*B*(5)	*Na*(1)	*Na*(2)	*Sr*	Σ	H(1)
O(1)	1.50						0.06		0.27	1.83	
O(2)	1.54						0.11			1.65	0.20
O(3)	1.42						0.13		0.26	2.00	
									0.19		
O(4)	1.56						0.18		0.08	1.82	
O(5)		0.80	0.79						0.25	1.84	
O(6)		0.75				1.06	0.12	0.16		2.09	
O(7)		0.73		0.99			0.13		0.24	2.09	
O(8)		0.72			0.99				0.18	2.06	
									0.17		
O(9)			0.78	1.02					0.19	1.99	
O(10)			0.75		1.08			0.20		2.03	
O(11)			0.73	1.00			0.06		0.21	2.00	
O(12)					0.93	0.98		0.17		2.08	
OH						0.99		0.15		1.25	0.80
								0.11			
W(1)							0.26	0.20		0.46	
W(2)										0.00	
Σ	6.02	3.00	3.05	3.01	3.00	3.03	1.05	0.99	2.04		1.00

(Brown & Altermatt 1985). *Na*(1) = $Na_{0.856}K_{0.144}$; *Sr* = $Sr_{0.822}Ca_{0.178}$

TABLE 9. COMPOUNDS BASED ON THE $[B_5O_8(OH)]$ SHEET

	Space Group	*a* (Å)	*b* (Å)	*c* (Å)	α (°)	β (°)	γ (°)	Ref.
Fontarnauite-type sheet								
fontarnauite, $Na_2Sr(SO_4)[B_5O_8(OH)](H_2O)_2$	$P2_1/c$	6.458	22.299	8.571	90	103.05	90	[1]
Biringuccite-type sheet								
biringuccite, $Na_2[B_5O_8(OH)](H_2O)$	$P2_1/c$	11.196	6.561	20.757	90	93.89	90	[2]
veatchite, $Sr_2(B(OH)_3)[B_5O_8(OH)]_2(H_2O)$	*Aa*	20.860	11.738	6.652	90	92.10	90	[3]
$Ba[B_5O_8(OH)](H_2O)$ [a]	$P\bar{1}$	6.781	6.901	9.737	102.55	91.51	119.72	[4]
$Ca[B_5O_8(OH)](H_2O)$	$P2_1/c$	6.530	19.613	6.530	90	119.21	90	[5]
$Pb[B_5O_8(OH)](H_2O)_{1.5}$	$P\bar{1}$	6.656	6.714	10.701	99.07	93.67	118.87	[6]
Nasinite-type sheet								
nasinite, $Na_2[B_5O_8(OH)](H_2O)_2$	$Pna2_1$	12.015	6.518	11.173	90	90	90	[7]
gowerite, $Ca(B(OH)_3)[B_5O_8(OH)](H_2O)$	$P2_1/a$	12.882	16.360	6.558	90	121.62	90	[8]
volkovskite, $KCa_4(B(OH)_3)_2[B_5O_8(OH)]_4(H_2O)_4$	$P1$	6.535	24.185	6.589	92.63	119.13	97.30	[9]
$Na_2[B_5O_8(OH)](H_2O)_2$	Pc	11.323	6.562	12.244	90	91.05	90	[10]
$Nd[B_5O_8(OH)](H_2O)_2$ I [b]	$P2_1/n$	6.476	15.350	10.673	90	90.32	90	[11]
$K_2[B_5O_8(OH)](H_2O)_2$	$Pna2_1$	12.566	6.671	11.587	90	90	90	[12]

[a] illustrated in Figure 16a

[b] illustrated in Figure 16b

References: [1] this work; [2] Corazza *et al.* (1974); [3] Clark & Christ (1971); [4] Belokoneva *et al.* (2008); [5] Yamnova *et al.* (2003); [6] Chen *et al.* (2006); [7] Corazza *et al.* (1975); [8] Konnert *et al.* (1972); [9] Poulin & Grice (2013); [10] Liu *et al.* (2006); [11] Polinski *et al.* (2012); [12] Marezio (1969).

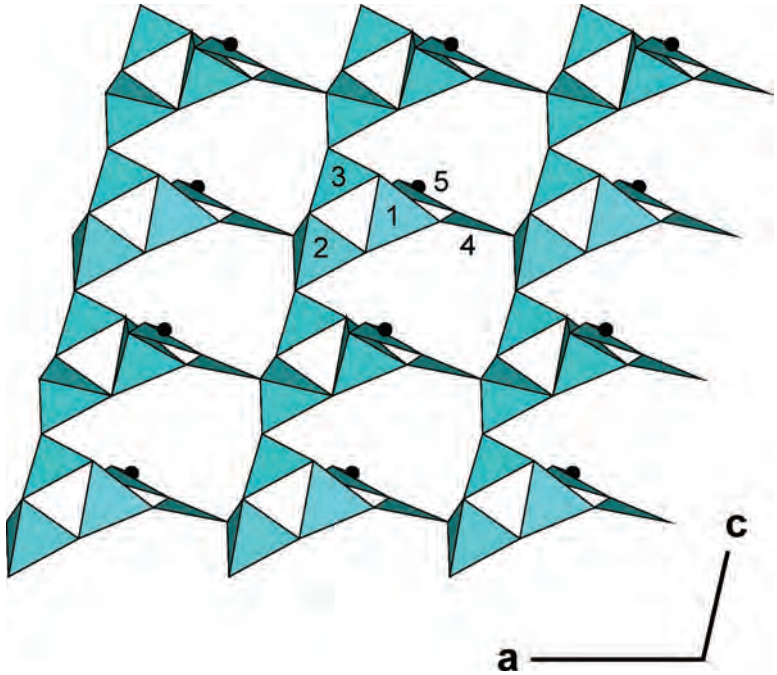

FIG. 12. The $[B_5O_8(OH)]$ sheet in fontarnauite projected down [010]. The B identities of a single $B_5O_{10}(OH)$ unit are labeled.

chemical composition (Fig. 9); neutrality is maintained with only univalent cations at *Na*(1) and *Na*(2), and only divalent cations occupying the *Sr* site. Moreover, near-ideal aggregate bond-valence sums result for the *Na*(1), *Na*(2), and *Sr* sites (Table 8). We thus conclude that the site-specific composition $(Na_{0.856}K_{0.144})^{Na(1)}Na^{Na(2)}(Sr_{0.822}Ca_{0.178})^{Sr}$ best represents the fontarnauite X-ray single-crystal; this composition is very close to the average results of the 43 individual chemical analyses.

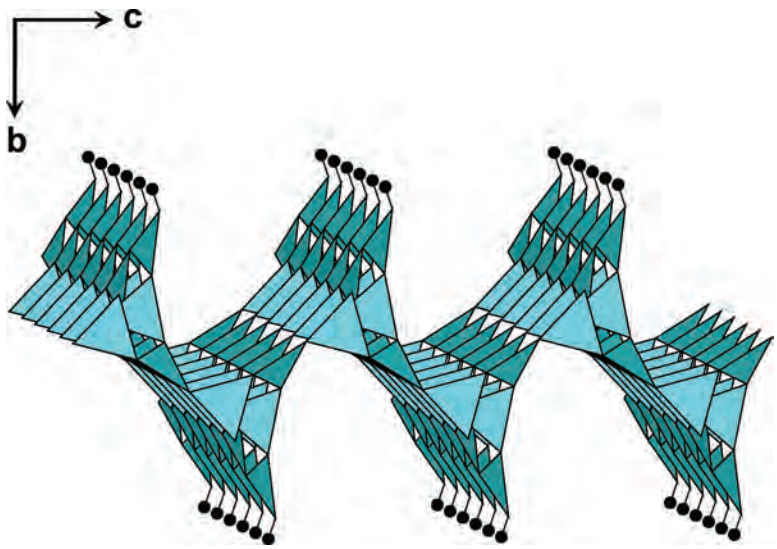

FIG. 13. A perspective view of the $[B_5O_8(OH)]$ sheet in fontarnauite projected down an axis rotated $\sim 5°$ from [100].

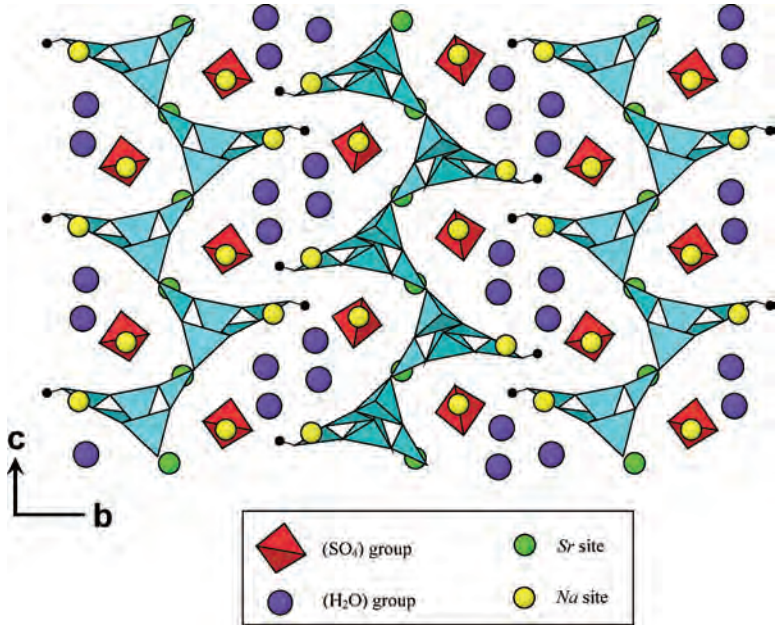

FIG. 14. The crystal structure of fontarnauite projected down [100]. Blue triangles and tetrahedra represent boron groups.

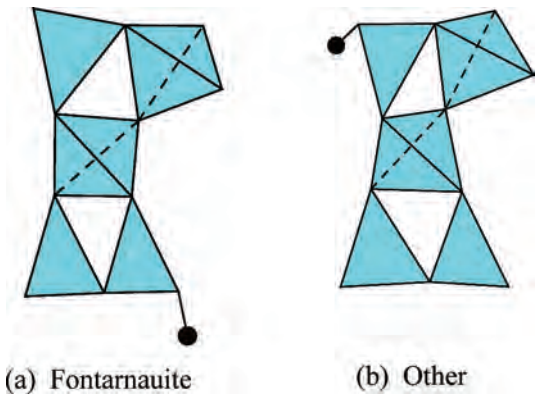

FIG. 15. The <2Δ□>–<Δ2□> FBB in (a) fontarnauite and (b) other related borates.

Crystal structure: description

In the structure of fontarnauite, two (BO_4) tetrahedra and three (BO_3) triangles share vertices to form $B_5O_{10}(OH)$ units (Fig. 11) that link to other $B_5O_{10}(OH)$ units along [100] and [001] to form a $[B_5O_8(OH)]$ sheet parallel to (010) (Fig. 12). The $[B_5O_8(OH)]$ sheet is highly corrugated, with $B_5O_{10}(OH)$ units alternately projecting up and down [010] along [001] within the sheet (Fig. 13). Opposing cusps in neighboring $[B_5O_8(OH)]$ sheets are slightly offset from each other near the terminal (OH) group (Fig. 14). Within the central cavities of opposing $[B_5O_8(OH)]$ sheets are the H_2O groups, SO_4 tetrahedra, and *Na*(1) sites; the *Sr* and *Na*(2) sites occur within the interstices of a given $[B_5O_8(OH)]$ sheet. Where opposing cusps of neighboring $[B_5O_8(OH)]$ sheets approach each other, there is extensive weak H-bonding associated with the (OH) and (H_2O) groups, in accord with the observed perfect {010} cleavage.

Structural relations to other species

The basic component in the fontarnauite structure is the $B_5O_{10}(OH)$ unit, comprised of three $B\Phi_3$ (Φ: unspecified anion) triangles and two $B\Phi_4$ tetrahedra that share vertices to form a three-membered $–B\Phi_3–B\Phi_3–B\Phi_4–$ ring and a three-membered $–B\Phi_3–B\Phi_4–B\Phi_4–$ ring, with a common $B\Phi_4$ tetrahedron shared between the two rings. Thus, the fundamental building block (FBB) in fontarnauite can be described as 3Δ2□ : <2Δ□>–<Δ2□> (Burns *et al.* 1995). There are five other minerals that also contain this FBB: nasinite, $Na_2[B_5O_8(OH)](H_2O)_2$, biringuccite, $Na_2[B_5O_8(OH)](H_2O)$, veatchite, $Sr_2(B(OH)_3)[B_5O_8(OH)]_2(H_2O)$, gowerite, $Ca(B(OH)_3)[B_5O_8(OH)](H_2O)$, and volkovskite, $KCa_4(B(OH)_3)_2[B_5O_8(OH)]_4(H_2O)_4$. In these structures, the <2Δ□>–<Δ2□> FBBs link to form $[B_5O_8(OH)]$ sheets (Hawthorne *et al.* 2002). The

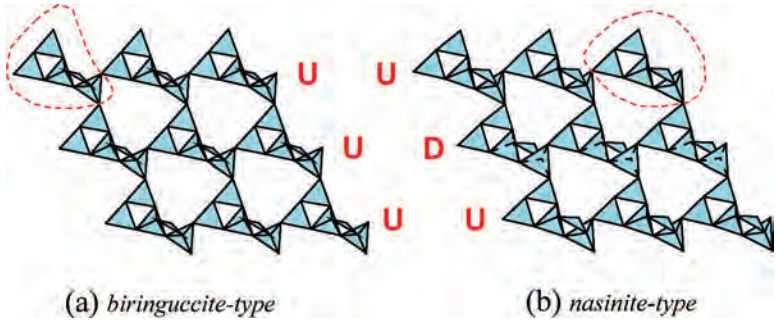

FIG. 16. The $[B_5O_8(OH)]$ configuration in (a) *biringuccite-type* sheets and (b) *nasinite-type* sheets. Red dashed lines enclose a single $B_5O_{10}(OH)$ cluster; U,D lettering denotes rows of $B_5O_{10}(OH)$ clusters, in which the BΦ3 groups not involved with linkage between clusters point up or down.

<2Δ□>–<Δ2□> FBB of fontarnauite is shown beside that of the other borates (nasinite, biringuccite, veatchite, gowerite, and volkovskite) in Figure 15. The basic topology is the same, but the FBBs differ in their absolute positioning of the (OH) group; in fontarnauite it is located on the right $B\Phi_3$ triangle of the $–B\Phi_3–B\Phi_3–B\Phi_4–$ ring (Fig. 15a); the (OH) group in all other related borates (minerals and synthetic compounds to date) is located on the $B\Phi_3$ triangle of the $–B\Phi_3–B\Phi_4–B\Phi_4–$ ring (Fig. 15b). As all of the anion vertices (except OH) of the <2Δ□>–<Δ2□> FBB are linked to two B atoms, the connectivities within the borate sheet in fontarnauite and the related minerals and compounds are fundamentally different.

The crystal structures of nasinite and biringuccite are both based on the same FBB shown in Figure 15b; however, the $[B_5O_8(OH)]$ sheet topologies differ in that the $B_5O_{10}(OH)$ units either all point in the same direction (*i.e.*, biringuccite) within a given sheet, or alternately point in opposing directions (*i.e.*, nasinite), and the two arrangements are referred to as geometrical isomers (Hawthorne 1983, 1985, Hawthorne *et al*. 2002). A search of the ICSD revealed three additional synthetic borate compounds with the *biringuccite-type* $[B_5O_8(OH)]$ sheet (Fig. 16a) and three with the *nasinite-type* $[B_5O_8(OH)]$ sheet (Fig. 7b) (Table 9). In comparing Figure 16 with Figure 13, we see that the crystal structure of fontarnauite, with a stereochemically different (OH) group on the $B_5O_{10}(OH)$ cluster, offers a new $[B_5O_8(OH)]$ sheet topology not previously reported for a mineral or synthetic compound.

Fontarnauite is not structurally related to any of the other borate-sulfate minerals for which structural information is available (Table 1). The most similar structure is that of heidornite, $Na_2Ca_3B_5O_8(OH)_2(SO_4)_2Cl$, in which the basic component, $B_5O_8(OH)_2$, is composed of two rings <Δ2□> linked through the triangle to form an FBB <Δ2□>–<Δ2□>, which are joined through a tetrahedron to form chains (Burzlaff 1967, Hawthorne *et al*. 2002). Three sulfate-borate minerals, buryatite, charlesite, and sturmanite, are members of the ettringite group, but only the structure of sturmanite has been refined (Pushcharovsky *et al*. 2004). Of the three other sulfate-borate minerals, the structures of sulfoborite (Giese & Penna 1983) and martinite (McDonald & Chao 2007) have been refined, whereas that of vitimite (Chukanov *et al*. 2002) has yet to be determined. Boron is present in both trigonal and tetrahedral coordinations in sturmanite, but only in tetrahedral coordination in the other two minerals; in all three minerals, the B polyhedra are isolated with no additional connectivity.

DEDICATION

John Jambor had eclectic interests that encompassed mine waste and new minerals, including sulfates, so the description of the new mineral fontarnauite, a borate-sulfate, is eminently appropriate for inclusion in an issue dedicated to John. Fontarnauite, only the eighth borate-sulfate to be discovered (Table 1), represents a commonality between our interest in borates and John's interests. In addition, ESG had the privilege to work for eight years with John on *New Mineral Names*, a thoroughly enjoyable introduction to the realm of mineral classification, and so he would like to have this description dedicated to John; FCH wishes to acknowledge a long friendship with John, he learned a lot from John when he was Editor of *The Canadian Mineralogist*.

ACKNOWLEDGMENTS

This study was supported by projects CGL2013-42689 and 2014-SGR 251 of the Spanish and Catalan

Governments, respectively. The Eti Mine Company (Turkey) is thanked for logistic support and permission to study core samples. The authors are grateful to the staff of the CCiTUB for their work in analytical determinations and to F. Ortí, L. Rosell, I. Gündoğan, I. Subias, and J. Illa for their valuable help. We thank Dr. José Manuel Astilleros, Director of the journal *Macla* for permission to use the figures previously published in *Macla*. Joel Grice, Robert Martin, and an anonymous reviewer are thanked for their constructive comments on an earlier version of the manuscript.

References

Bastin, G.F. & Heijligers, H.J.M. (2000) Quantitative electron probe microanalysis of boron. *Journal of Solid State Chemistry* **154**, 177–187.

Belokoneva, E.L., Stefanovich, S.Y., Erilov, M.A., Dimitrova, O.V., & Mochenova, N.N. (2008) A new modification of $Ba[B_5O_8(OH)]\cdot H_2O$, the refined structure of $Ba_2[B_5O_9]Cl\cdot 0.5H_2O$, and the role of the pentaborate structural units in the formation of the quadratic optical nonlinearity. *Crystallography Reports* **53**, 228–236.

Brown, I.D. & Altermatt, D. (1985) Bond-valence parameters obtained from a systematic analysis of the inorganic crystal structure database. *Acta Crystallographica* **B41**, 244–247.

Bücking, H. (1893) Sulfoborit, ein neues krystallisirtes Borat von Westeregeln. *Sitzungsberichte der Königlich Preussischen Akademie der Wissenschaften zu Berlin* **1893**, 967–972.

Burns, P.C., Grice, J.D., & Hawthorne, F.C. (1995) Borate minerals I. Polyhedral clusters and fundamental building blocks. *Canadian Mineralogist* **33**, 1131–1151.

Burzlaff, H. (1967) Die Struktur des Heidornit $Ca_3Na_2Cl(SO_4)_2B_5O_8(OH)_2$. *Neues Jahrbuch für Mineralogie Monatshefte*, 157–169.

Cairncross, B. & Beukes, N.J. (2013) *The Kalahari Manganese Field. The Adventure Continues*. Struik Nature, Cape Town, South Africa, 384 pp.

Chen, X., Zhao, Y., Chang, X., Zuo, J., Zang, H., & Xiao, W. (2006) Synthesis and crystal structures of two new hydrated borates, $Zn_8[(BO_3)_3O_2(OH)_3]$ and $Pb[B_5O_8(OH)]\cdot 1.5H_2O$. *Journal of Solid State Chemistry* **179**, 3911–3918.

Chukanov, N.V., Pekov, I.V., Malinko, S.V., Zadov, A.E., & Dubinchuk, V.T. (2002) Vitimite, $Ca_6B_{14}O_{19}[SO_4](OH)_{14}\cdot 5H_2O$, a new mineral, and conditions of its formation in Solongo deposit, Buryatia. *Zapiski Vserossiyskogo Mineralogicheskogo Obshchestva* **131(4)**, 41–46 (in Russian).

Clark, J.R. & Christ, C.L. (1971) Veatchite: crystal structure and correlations with p-veatchite. *American Mineralogist* **56**, 1934–1954.

Corazza, E., Menchetti, S., & Sabelli, C. (1974) The crystal structure of biringuccite, $Na_4[B_{10}O_{16}(OH)_2]\cdot 2H_2O$. *American Mineralogist* **59**, 1005–1015.

Corazza, E., Menchetti, S., & Sabelli, C. (1975) The crystal structure of nasinite, $Na_2[B_5O_8(OH)]\cdot 2H_2O$. *Acta Crystallographica* **B31**, 2405–2410.

Dunn, P.J., Peacor, D.R., Leavens, P.B., & Baum, J.L. (1983) Charlesite, a new mineral of the ettringite group, from Franklin, New Jersey. *American Mineralogist* **68**, 1033–1037.

García-Veigas, J., Rosell, L., Alcobé, X., Subias, I., Ortí, F., Gündoğan, I., & Helvaci, C. (2010) Fontarnauite, a new sulphate-borate mineral from the Emet borate District (Turkey). *Macla* **13**, 97–98.

García-Veigas, J., Rosell, L., Ortí, F., Gündoğan, İ., & Helvaci, C. (2011) Mineralogy, diagenesis and hydrochemical evolution in a probertite–glauberite–halite saline lake (Miocene, Emet Basin, Turkey). *Chemical Geology* **280**, 352–364.

Giese, R.F., Jr. & Penna, G. (1983) The crystal structure of sulfoborite, $Mg_3SO_4(B(OH)_4)_2(OH)F$. *American Mineralogist* **68**, 255–261.

Hawthorne, F.C. (1979) The crystal structure of morinite. *Canadian Mineralogist* **17**, 93–102.

Hawthorne, F.C. (1983) Enumeration of polyhedral clusters. *Acta Crystallographica* **A39**, 724–736.

Hawthorne, F.C. (1985) Towards a structural classification of minerals: the $^{VI}M^{IV}T_2\Phi_n$ minerals. *American Mineralogist* **70**, 455–473.

Hawthorne, F.C. (2012) A bond-topological approach to theoretical mineralogy: crystal structure, chemical composition and chemical reactions. *Physics and Chemistry of Minerals* **39**, 841–874.

Hawthorne, F.C. (2014) The structure hierarchy hypothesis. *Mineralogical Magazine* **78**, 957–1027.

Hawthorne, F.C., Cooper, M., Bottazi, P., Ottolini, L., Ercit, T.S., & Grew, E.S. (1995a) Micro-analysis of minerals for boron by SREF, SIMS and EMPA: a comparative study. *Canadian Mineralogist* **33**, 389–397.

Hawthorne, F.C., Ungaretti, L., & Oberti, R. (1995b) Site populations in minerals: terminology and presentation of results of crystal-structure refinement. *Canadian Mineralogist* **33**, 907–911.

Hawthorne, F.C., Krivovichev, S.V., & Burns, P.C. (2000) The crystal chemistry of sulfate minerals. *In* Sulfate Minerals: Crystallography, Geochemistry and Environmental Significance (C.N. Alpers, J.L. Jambor, & D.K. Nordstrom, eds.). *Reviews in Mineralogy and Geochemistry* **40**, 1–112.

Hawthorne, F.C., Burns, P.C., & Grice, J.D. (2002) The crystal chemistry of boron. *In* Boron Mineralogy, Petrology and Geochemistry (second printing) (E.S. Grew & L.M. Anovitz, eds.). *Reviews in Mineralogy* **33**, 41–115.

Helvaci, C. (1986) *Stratigraphic and structural evolution of the Emet borate deposits, Western Anatolia, Turkey*. Research paper MM/JEO-86, Dokuz Eylül Üniversitesi, Izmir, Turkey, 28 pp.

Helvaci, C. & Alonso, R.N. (2000) Borate deposits of Turkey and Argentina; a summary and geological comparison. *Turkish Journal Earth Sciences* **9**, 1–27.

Helvaci, C. & Ortí, F. (1998) Sedimentology and diagenesis of Miocene colemanite-ulexite deposits (western Anatolia, Turkey). *Journal of Sedimentary Research* **68**, 1021–1033.

International Centre for Diffraction Data (2012) *PDF-2; PDF-4 Powder Diffraction File*. ICDD, Newton Square, Pennsylvania, United States, <http://www.icdd.com>.

Konnert, J.A., Clark, J.R., & Christ, C.L. (1972) Gowerite, $CaB_5O_8(OH)\cdot B(OH)_3\cdot 3H_2O$: crystal structure and comparison with related borates. *American Mineralogist* **57**, 381–396.

Le Bail, A., Duroy, H., & Fourquet, J.L. (1988) *Ab initio* structure determination of $LiSbWO_6$ by X-ray powder diffraction. *Materials Research Bulletin* **23**, 447–452.

Li, J., Xia, S.-P., & Gao, S.-Y. (1995) FT-IR and Raman spectroscopic study of hydrated borates. *Spectrochimica Acta* **A51**, 519–532.

Liu, Z.H., Li, L.Q., & Wang, M.Z. (2006) Synthesis, crystal structure and thermal behavior of $Na_4[B_{10}O_{16}(OH)_2]\cdot 4H_2O$. *Journal of Alloys and Compounds* **407**, 334–339.

Lobanova, V.V. (1958) Sulfoborite in salt deposits of the Caspian depression and the southern Urals. *Doklady Akademii Nauk SSSR* **122**, 905–908 (in Russian).

Louër, D. & Boultif, A. (2006). Indexing with the successive diochotomy method. DICVOL04. *Zeitschrift für Kristallographie* **23**, 225–230.

Malinko, S.V., Chukanov, N.V., Dubinchuk, V.T., Zadov, A.E., & Koporulina, Ye.V. (2001) Buryatite, $Ca_3(Si,Fe^{3+},Al)SO_4[B(OH)_4](OH)_5O\cdot 12H_2O$, a new mineral. *Zapiski Vserossiyskogo Mineralogicheskogo Obshchestva* **130(2)**, 72–78 (in Russian).

Marezio, M. (1969) The crystal structure of $K_2[B_5O_8(OH)]\cdot 2H_2O$. *Acta Crystallographica* **B25**, 1787–1795.

McDonald, A.M. & Chao, G.Y. (2007) Martinite, a new hydrated sodium calcium fluorborosilicate species from Mont Saint-Hilaire, Quebec: description, structure determination and genetic implications. *Canadian Mineralogist* **45**, 1281–1292.

McGee, J.J., Slack, J.F., & Herrington, C.R. (1991) Boron analysis by electron microprobe using MoB_4C layered synthetic crystals. *American Mineralogist* **76**, 681–684.

Menchetti, S., Sabelli, C., & Trosti-Ferroni, R. (1982) Probertite, $CaNa[B_5O_7(OH)_4]\cdot 3H_2O$: a refinement. *Acta Crystallographica* **B38**, 3072–3075.

Ortí, F., Helvaci, C., Rosell, L., & Gündoğan, İ. (1998) Sulphate-borate relations in an evaporitic lacustrine environment: the Sultançayır Gypsum (Miocene, western Anatolia). *Sedimentology* **45**, 697–710.

Peacor, D.R., Dunn, P.J., & Duggan, M. (1983) Sturmanite, a ferric iron, boron analogue of ettringite. *Canadian Mineralogist* **21**, 705–709.

Pekov, I.V. & Abramov, D.V. (1993) Boron deposit of the Inder and its minerals. *World of Stones* **1**, 23–30.

Polinski, M.J., Wang, S., Cross, J.N., Alekseev, E.V., Depmeier, W., & Albrecht-Schmitt, T.E. (2012) Effects of large halides on the structures of lanthanide(III) and plutonium(III) borates. *Inorganic Chemistry* **51**, 7859–7866.

Pouchou, J.L. & Pichoir, F. (1988) Determination of mass absorption coefficients for soft X-rays by use of the electron microprobe. *In* Microbeam Analysis (D.E. Newbury, ed.). San Francisco Press, San Francisco, California, United States (319–324).

Poulin, R.S. & Grice, J.D. (2013) Volkovskite, a complex borate mineral: refined crystallographic data and optics. *Canadian Mineralogist* **51**, 157–169.

Pushcharovsky, D.Yu., Lebedeva, Yu.S., Zubkova, N.V., Pasero, M., Bellezza, M., Merlino, S., & Chukanov, N.V. (2004) The crystal structure of sturmanite. *Canadian Mineralogist* **42**, 723–729.

Rodriguez-Carvajal, J. (1997) *Journées de la Diffusion Neutronique, Ecole Thematique Cristallographie et Neutrons*, May 1997, Batz sur Mer, France. <ftp://charybde.saclay.cea.fr/pub/divers/fullp/doc/fpjdn.ps>.

Schindler, M. & Hawthorne, F.C. (2001a) A bond-valence approach to the structure, chemistry and paragenesis of hydroxy-hydrated oxysalt minerals: I. Theory. *Canadian Mineralogist* **39**, 1225–1242

Schindler, M. & Hawthorne, F.C. (2001b) A bond-valence approach to the structure, chemistry and paragenesis of hydroxy-hydrated oxysalt minerals: II. Crystal structure and chemical composition of borate minerals. *Canadian Mineralogist* **39**, 1243–1256.

Schindler, M. & Hawthorne, F.C. (2001c) A bond-valence approach to the structure, chemistry and paragenesis of hydroxy-hydrated oxysalt minerals: III. Paragenesis of borate minerals. *Canadian Mineralogist* **39**, 1257–1274.

Shannon, R.D. (1976) Revised effective ionic radii and systematic studies of interatomic distances in halides and chalcogenides. *Acta Crystallographica* **A32**, 751–767.

Sheldrick, G.M. (2008) A short history of SHELX. *Acta Crystallographica* **A64**, 112–122.

Siemroth, J. (2008) Das Vorkommen von Boratmineralen im Werra-Anhydrit des Steinbruchs Kohnstein bei Niedersachswerfen am Südharz. *Aufschluss* **59**, 353–366.

von Engelhardt, W., Füchtbauer, H., & Zemann, J. (1956) Heidornit $Na_2Ca_3[Cl•(SO_4)_2•B_5O_8(OH)_2]$ ein neues Bormineral aus dem Zechsteinanhydrit. *Heidelberger Beiträge zur Mineralogie und Petrographie* **5**, 177–186.

Yamnova, N.A., Egorov-Tismenko, Y.K., Zubkova, N.V., Dimitrova, O.V., Kantor, A.P., Danian, Y., & Ming, X. (2003) Crystal structure of new synthetic calcium pentaborate $Ca[B_5O_8(OH)]·H_2O$ and its relation to pentaborates with similar boron-oxygen radicals. *Crystallography Reports* **48**, 557–562.

Received November 5, 2014. Revised manuscript accepted January 21, 2015.